Journal of Engineering and Technology for Industrial Applications

ITEGAM-JETIA

Manaus, v.11 n.55, p. 238-249. September/October, 2025.

DOI: https://doi.org/10.5935/jetia. v.11 n.55.2673.

ISSN ONLINE: 2447-0228

RESEARCH ARTICLE OPEN ACCESS

INVESTIGATION OF PARTIAL DEMAGNETIZATION FAULTS IN PERMANENT MAGNET SYNCHRONOUS MOTORS BASED ON EFFICIENCY AND LOSS MAPS ADVANCED ANALYSIS

Layachi Chebabhi[1], Toufik Tayeb Naas[2], Mohamed Zitouni[3], Monaem Elmnifi[4], and Abdelkarim Cherhabil[5]

[1] Laboratory of Applied Automation and Industrial Diagnostics (LAADI), Department of Mechanical Engineering in the Faculty of Science and Technology, Ziane Achour University of Djelfa, PO Box 3117, Djelfa 17000, Algeria.

[2,3] Laboratory of Gas Turbine Joint Research Team, Department of Mechanical Engineering in the Faculty of Science and Technology, Ziane Achour University of Djelfa, PO Box 3117, Djelfa 17000, Algeria.

[4] Department of Mechanical Engineering Technology, FSBEI "Belgorod State Technological University named after. V.G. Shukhov." 308012, Belgorod, st. Kostyukova 46. Russia.

[5] Laboratoire de Modélisation Simulation et Optimisation des Systèmes Complexes Réels, Department of Electronics and Communications, Ziane Achour University of Djelfa, PO Box 3047, Ain Chih, Djelfa, 17000, Algeria.

[1]https://orcid.org/0009-0002-4451-8533, [2]http://orcid.org/0000-0002-5539-6415, [3]https://orcid.org/0009-0003-3088-7431, [4]http://orcid.org/0000-0003-4074-1877, [5]http://orcid.org/0009-0006-1437-1453

Email: layachi.chebabhi@univ-djelfa.dz, t.naas@univ-djelfa.dz, mohamed.zitouni@gmail.com, monm.hamad@Yahoo.co.uk, Abdelkarim.cherhabil@univ-djelfa.dz

ARTICLE INFO

Article History

Received: September 5, 2025

Revised: September 30, 2025

Accepted: October 7, 2025

Published: October 31, 2025

Keywords:

Demagnetization,
Permanent Magnet Synchronous Motors,
Electromagnetic Analysis,
Efficiency Maps.

ABSTRACT

Demagnetization failure is a critical and prevalent fault in interior permanent magnet synchronous motors (IPMSMs), resulting from a variety of factors including thermal overheating, high electrical currents, and mechanical vibrations. Although the electromagnetic analysis and performance curves provides a deep insight into the machine behavior, it is not able to emulate the actual performance under various operating loads. To tackle these restrictions, advanced analytical tools such as efficiency maps are adopted to predict the behavior more accurately, which allows for enhanced performance monitoring. This paper aimed to incorporate electromagnetic analysis with efficiency maps to investigate the IPMSMs partial demagnetization fault, with emphasis on the magnetic flux residual density coefficient (Br) variations. The results indicated a significant degradation in the performance after exposure to the fault, with a 57% decrease in the generated torque, losses increased up to 35%, with a significant reduction in the range of high efficiency areas greater than 70% over the efficiency maps, and a deterioration in the efficiency especially at low speeds as the peak torque range is reduced. This study provides a comprehensive framework for evaluating the demagnetization faults effection, thus contributing to the elaboration of effective operation and maintenance strategies.

I. INTRODUCTION

IPMSMs are used in electromechanical power conversion technologies in high performance applications, dominating the sectors of traction systems for electric and hybrid vehicles [1-3], renewable energy systems for wind turbines as part of grid conversion systems [4,5], photovoltaic to mechanical energy conversion systems [6,7], advanced industrial automation platforms, Maglev high speed trains [8], electric aircraft and unmanned aerial vehicles (UAVs) [9,10], Distributed propulsion control systems [11], high resolution automated production lines, electric submarines, smart ships, and unmanned underwater vehicles (UUVs) [12-14].

The features of these machines include high power density, which allows reducing size and weight compared to other machines with the same power, constant speed range, low losses and efficiency up to 95% owing to the existence of internal magnets, the ability of operating in a wide range of speeds without significant losses and generate high torque which makes them suitable for rapid start up in electric vehicles [15], and the possibility of precise torque and speed control and compatibility with advanced control technologies such as direct torque control (DTC) and field oriented control (FOC) [16,17], Extended permanent magnet service lifetime and homogeneous flux distribution inside the rotor that eliminates magnet direct thermal conductivity, efficient dynamic performance and rapid response to load and transients that reduces noise and vibration. The operational reliability of permanent magnet synchronous motors (PMSM) systems is mainly related to the integrity of the permanent magnet magnetic field , despite the superior materials properties, they are susceptible to demagnetization effects under extreme operational conditions, which constitutes a critical failure mode that affects both operational safety and long term system performance.

Demagnetization is a complex degradation mechanism that involves an irreversible or quasi reversible decrease in the flux density of a permanent magnet. This failure occurs through a variety of methods including heat induced demagnetization when operating temperatures exceed the magnet's curie temperature [18] or approach critical thermal limits, demagnetization caused due to the exposure to adverse magnetic fields that exceed strength limits, and mechanical demagnetization caused due to the occurrence of structural stresses and vibrations. Industry researchs indicates that partial demagnetization, which can affect more than 10% of the magnetic field strength, leads to a 5-25% reduction in torque [19], a decrease in efficiency, and significant changes in the characteristics of electromagnetic torque. Whereas total demagnetization, although rare leads to a complete loss of torque capability and system failure. Predictive maintenance is considered an important direction in the PMSM maintenance field, where studies [20,21] have developed advanced methods and techniques for predicting failures before their occurrence through monitoring electrical and mechanical signals and operational indicators. These techniques aim to reduce costs and enhance operational efficiency through pre-planned maintenance.

Several designs of IPMSMs have been proposed for enhancing performance and improve the operational efficiency, where researchs [22-24] focused on improving the machines structures, permanent magnet geometry and its distribution inside the rotor to achieve higher power efficiency, speed and torque properties to reduce harmonic distortion and magnetic losses and to reduce vibration and torque ripples. Electromagnetic analysis contributes to the advanced analysis of the behavior and determination of areas of magnetic flux concentration precisely, the effect of magnetic saturation, and iron loss on electric motors [24-26]. Previous researches have investigated several important aspects of IPMSMs, focusing on analysis of various fault types and their direct impact on the performance and operating efficiency in [27-31]. The broken permanent magnets failure of and its impacts on the mechanical and electrical behavior of the PMSM were presented in [32], while researches [33,34] have focused on the analysis of acoustic noises and electromagnetic vibration generated during operation and their impact on overall PMSM performance. A demagnetization fault diagnosis method for PMSM based on machine learning (ML) was proposed by applying time frequency domain analysis and short time fourier transform (STFT) in detecting permanent magnet faults through stator phase current signal analysis [35].

In [36], the method of using acoustic signals for detection in the diagnosis of demagnetization and deflection faults of PMSM was investigated by feature conversion into 2D images, and fault detection and classification by a DeiT classifier was examined. The accuracy of the proposed method reaches 99.26%, demonstrating the reliability and effectiveness of the method. The thermal behavior of the interior permanent magnet synchronous motor (IPMSM) local demagnetization fault was discussed, adding temperature to the input signals to diagnose the demagnetization fault through back propagation neural network, predicting the healthy state of the permanent magnet, and determining the demagnetization ratio as an output signal [37]. LSTM and GRU neural network models were adopted for fault classification and early detection of demagnetization and short circuit in the PMSM based on the three current signals of different operating states of the motor, the two methods showed a high accuracy of about 98.7% in detecting faults [38]. A technique has been proposed that allows accurate localization of demagnetized permanent magnets in PMSM. This method adopts three toroidal yoke coils, which are used to measure the Back EMF. They are coiled in the stator core and through waveform analysis, the location of the fault can be determined [39].

A method for identifying and detecting the location of demagnetization faults in PMSM by analyzing the sub-current signal and calculating the pearson correlation coefficient between modeled and real currents was introduced, which provides an accurate and non-intrusive method for determining the location and level of fault [40]. A method that relies on the combination of neural convolutional networks (CNN) and gramian angular fields (GAF) transformation was proposed to classify and identify various demagnetization faults, based on the output torque signal with a model training accuracy of 98.33% and a test accuracy of 97.41% [41]. The impact of inclined magnetic fields on the partial demagnetization in NdFeB magnets is investigated through proposing a model that relies on an exponential function to predict this behavior [42]. In [43], a novel method has been proposed that is distinguished with its ability to detect and accurately locate the fault based on time signal analysis without requiring complex analysis, relying on the Back EMF constant using a new search coil to diagnose the partial demagnetization fault in IPMSMs, while in [44] a real time fault diagnosis method has been proposed based on Kurtosis analysis of the magnetic flux density variation in the air gap with the use of frozen permeability technique and equivalent magnetic circuit model (EMC).

A method for demagnetization fault diagnosis using multi-parameter estimation and Dual Extended Kalman Filter (Dual EKF) using a least squares algorithm is presented, this method allows real time magnetic flux monitoring , and accurate fault diagnosis with an error ratio less than 5% [45]. While current diagnostic approaches rely on existing post-failure detection methodologies, which limits their benefit in adaptive control and predictive maintenance strategies, experimental investigations have focused on failure injection and rapid aging tests, which provide valuable insights into demagnetization mechanisms but remain limited in scale due to time requirements and cost constraints. Recent analytical modeling approaches have used electromagnetic, mechanical, and thermal analyses to predict the effects of demagnetization, but these techniques typically involve simplifying assumptions, limiting their accuracy in complex engineering structures and different operational conditions. Although previous studies have focused on presenting electromagnetic analyses of IPMSMs and various curves of the performance evaluation for demagnetization faults, it is very important

to adopt advanced predictive analytics to evaluate the behavior under various operating conditions over a wide range of speeds. The aim of this study is to use predictive analysis for demagnetization faults by combining efficiency and loss maps as well as electromagnetic analysis of different magnetic fields for more thorough evaluation of the machines behavior.

The main contributions of this study include the enhancement of an analytical framework for demagnetization fault by relying on high resolution electromagnetic simulation results with a focus on the efficiency and loss map analysis, the implementation of detailed finite element modeling to simulate the demagnetization fault and compare it with a healthy IPMSM, and the quantification of efficiency map variations under the demagnetization.This analysis uses a pure approach using experimental data obtained from simulation results with the ANSYS Maxwell to solve and analyze electromagnetic fields. Efficiency maps are a effective tool for advanced performance characterization of the IPMSMs, providing a thorough analysis of efficiency and loss distributions across different operating speed and torque ranges. Finite Element Analysis (FEA) has the ability to simplify complex engineering models in a short duration and a superior ability to capture detailed electromagnetic phenomena. Which makes it a popular choice for application in many areas of electrical engineering.

II. APPROACHED DESIGN OF THE IPMSM

This study aims to establish a simulation model for advanced analysis of the partial demagnetization faults in IPMSMs through exploiting advanced predictive analysis techniques using efficiency and loss maps. The prototype of the proposed machine was created with the ANSYS RMxprt tool, under the following operating conditions: voltage of 220 V, speed of 1800 rpm, and power of 550 watts. For the core components, high grade materials were selected, with M19_24G for the stator, copper as a conductor, and NdFeB as a permanent magnet. After a thorough analysis of the 2D prototype, the evaluation of various curves, and advanced electromagnetic analysis, the acquired data and results were used to compute and create the efficiency maps across a wide range of speed and torque variation. To study the demagnetization faults with a particular focus on the residual magnetic flux density (Br), and comparing the results with healthy IPMSM to assess the impact of this fault on the overall system behavior. The ANSYS Maxwell approach is based on the application of the finite element technique as the basis for numerical analysis to simplify various geometrical models and translate them into solvable systems with high efficiency, with the ability to provide accurate and fast solutions to complex designs.

Table 1: Parameters of the presented IPMSM.

Parameters	Evaluated Value
Outer Diameter of Stator (mm):	120
Inner Diameter of Stator (mm):	75
Number of Slots:	24
Outer Diameter of Rotor (mm):	74
Inner Diameter of Rotor (mm):	26
Length of Stator Core (mm):	65
Type of Steel:	M19_24G
Conductor Type:	copper_75C
Number of Rotor Poles:	4
Rated Output Power (kW):	550
Rated Voltage (V):	220
Given Rated Speed (rpm):	1800
Operating Temperature (C):	75

Source: Authors, (2025).

Table 2: Parameters of the IPMSM Pole.

Name	Evaluated Value
D1	72mm
O1	3mm
O2	3mm
B1	4mm
Rib	3mm
HRib	3mm
Layers	1
Magnet Thickness	5mm
Magnet Width	40mm
Magnet Type	NdFeB (N38)

Source: Authors, (2025).

III. DEMAGNETIZATION FAULT IN THE IPMSM

Permanent magnets are relied on to generate the magnetic field required for the operation of the IPMSM. Demagnetization is a gradual or abrupt process that leads to the permanent magnets to lose their magnetic strength, which decreases the machine's efficiency. It occurs as a result of several complex electrical and physical factors. Among the causes of the demagnetization are thermal factors when permanent magnets are exposed to high temperatures, there occur alterations in the structure of the magnetic material which reduces the overall magnetic power and affects the internal magnetic fields leading to a reduction in the coercivity and increases the potential for irreversible demagnetization to occur. High electric currents, particularly at overloads or short circuits, lead to the

generation of strong magnetic fields that oppose the normal magnetic field of the permanent magnet and may exceed the strength of the magnetic resistance, causing a partial or complete demagnetization. Mechanical shocks and recurring high vibrations can affect the permanent magnet's structure, causing a gradual deterioration of its magnetic properties. Demagnetization can be achieved by adjusting the properties of the materials. Magnetic effects can be reduced or eliminated by assigning passive non-magnetic properties to the material used, such as setting the magnetic permeability value to transition to a non-magnetic state or by adjusting the permanent magnet field. The demagnetization fault can be monitored through indicators such as voltage, torque, currents, and magnetic field analysis of flux density.

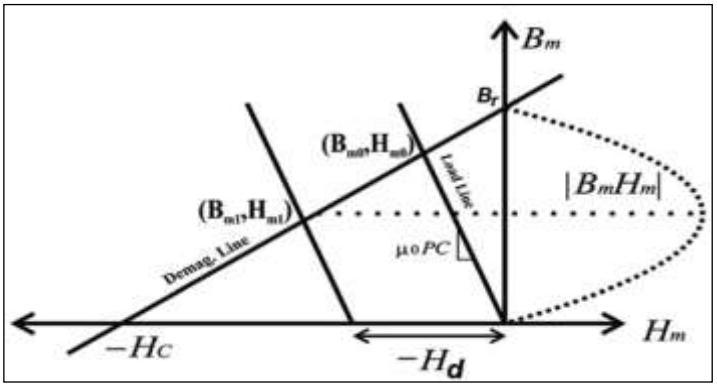

Figure 1: The characteristic of B-H demagnetisation of the permanent magnet.
Source: Taken from [46,47].

The no-load operating point is the intersection point of the B–H characteristic of the second quadrant (B-H demagnetization characteristics) at the load line and operating temperature, as illustrated in Figure 1. The load line slope relies on the permittivity coefficient PC [47] and is calculated by:

$$PC = -\frac{B_m}{\mu_0 H_m} = \frac{1}{f_{lkg}} \times \frac{A_g l_m}{A_m l_g} \tag{1}$$

where, the area of the air gap A_g equals the area of the magnet surface A_m, f_{lkg} is the different coefficient of the rotor leakage, l_g is the air-gap length. Therefore, the no-load operating (B_{m0}, H_{m0}) of the magnets are defined by:

From [46,47], the operating point of the no-load magnet (B_{m0}, H_{m0}), As illustrated in Figure 1, as follows:

$$B_{m0} = \frac{PC}{\mu_{rec} + PC} \times B_r$$
$$H_{m0} = \frac{B_r - B_{m0}}{\mu_{rec}\mu_0} \tag{2}$$

Where the magnet relative permeability is expressed as: $\mu_{\text{rec}} = \frac{B_r}{-\mu_0 H_c}$ [47].

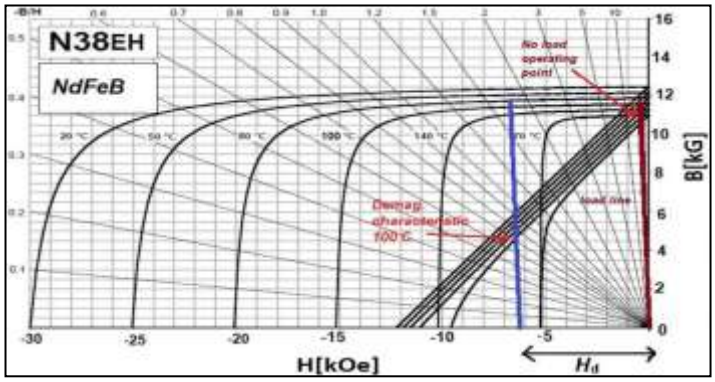

Figure 2: The NdFeB (N38EH) magnet demagnetisation B-H curves at various temperatures (1 kOe = 79.6 kA/m and 1 kG = 0.1 T).
Source: Taken from [48].

IV. FINITE ELEMENT ANALYSIS (FEA)

The finite element analysis (FEA) provides effectiveness in solving complex engineering systems. This method relies on numerical techniques to analyze complex engineering and physical systems that are difficult to solve with conventional analytical methods. The FEA divides geometric elements into a large number of small elements of a specific shape such as tetrahedrons and triangles connected to each other by a set of nodes, which facilitates and allows the application of mathematical equations on the elements to determine the overall system response in electrical machines. The machine parts are divided into very small elements,

which enables the magnetic fields to be separately modeled after being combined to obtain more accurate results and solve Maxwell's electromagnetic equations with high precision for each element as it contributes to solving the partial differential equations of magnetic fields for the flux density, eddy currents, mechanical ,and thermal in the electrical machine that is able to simplify the handling of heterogeneous materials and complex structures, as it contributes to accurately analysis of the flux, determine the parts exposed to magnetic saturation, anticipate the parts that are more prone to failures, and analysis of the dimensional and material variations effect based on simulation results leads to a reduction in the requirement to manufacturing many real models, which saves time and costs.

V. MATHEMATICAL MODELING OF THE IPMSM

A thorough analysis of the dynamic structure of the PMSM and the determination of the main factors that affect its functioning involves the use of scientific mathematical models that reveal the interdependence between different parameters such as torque, efficiency, loss, and power. These models provide the conceptual framework for the electromagnetic analysis and interpretation of experimental data extracted from the simulation. These equations are crucial for visualizing the mechanisms of power conversion and assessing the impact of external factors on the machine operational behavior. They allow for the analysis of the complicated interactions between magnetic fields and mechanical motion, enabling an accurate interpretation of the dynamic response of the machine in a variety of operating conditions. It also includes the evaluation of the design factors' impact on the operational properties.

Applying the Park transformation on the PMSM equation system, all current, voltage and flux vectors can be described in a rotor frame of reference [49-50]. Electrical equations of voltage in the d-q axis :

$$\begin{cases} V_d = R_s \cdot I_d + \frac{d\phi_d}{dt} - \omega_r \cdot \phi_q \\ V_q = R_s \cdot I_q + \frac{d\phi_q}{dt} + \omega_r \cdot \phi_d \end{cases} \tag{3}$$

Where $\omega_r = p.\Omega$ is the rotational electrical speed.

The magnetic flux in the d-q axis can be expressed by the formula below:

$$\phi_d = L_d \cdot I_d + \phi_f \tag{4}$$

$$\phi_q = L_q, I_q \tag{5}$$

Where ϕ_f is the field constant due to the permanent rotor excitation.

By replacing the Equations (4) and (5) in the Voltage Equation (3), this gives :

$$\begin{cases} V_d = R_s \cdot I_d + L_d \cdot \frac{di_d}{dt} - \omega_r \cdot L_q \cdot I_q \\ V_q = R_s \cdot I_q + L_q \cdot \frac{di_q}{dt} + \omega_r \cdot \left(L_d \cdot I_d + \phi_f\right) \end{cases} \tag{6}$$

Hence, the vector of the armature currents is expressed in the d-q axis as follows:

$$\begin{cases} \frac{dI_d}{dt} = -\frac{R_s}{L_d} \cdot I_d + \omega_r \cdot \frac{L_q}{L_d} \cdot I_q + \frac{1}{L_d} \cdot V_d \\ \frac{dI_q}{dt} = -\omega_r \cdot \frac{L_d}{L_q} \cdot I_d - \frac{R_s}{L_q} \cdot I_q + \frac{1}{L_q} \cdot V_q - \frac{1}{L_q} \cdot \phi_f \cdot \omega_r \end{cases} \tag{7}$$

Electromagnetic torque is defined by the partial derivative of the electromagnetic power with regard to the rotational angle of the rotor. This is given by :

$$T_e = \frac{dW_e}{d\theta_{geo}} = p \cdot \frac{dW_e}{d\theta} \tag{8}$$

Where W_e indicates the energy stored in the air-gap magnetic circuit, p is the number of pairs poles, θ_{geo} is the angular deviation of the moving part, expressed as follows: $\theta_{geo} = \frac{\theta_{\text{ele}}}{r}$.

The power expression is described as follows:

$$P(t) = \frac{3}{2}\left(V_d \cdot I_d + V_q \cdot I_q\right) \tag{9}$$

The d-q voltage Equation (3) are replaced in Equation (9) to obtain :

$$P(t) = \frac{3}{2}\left[R_s\left(I_d^2 + I_q^2\right)\right] + \frac{3}{2}\left[I_d \cdot \frac{d\phi_d}{dt} + I_q \cdot \frac{d\phi_q}{dt}\right] + \frac{3}{2}\left[\phi_d \cdot I_d - \phi_q \cdot I_q\right] \tag{10}$$

Where, the first expression (i.e., $\frac{3}{2}\left[R_s\left(I_d{}^2 + I_q{}^2\right)\right]$) represents the joule effect losses, the second term (i.e., $\frac{3}{2}\left[I_d \cdot \frac{d\phi_{\text{ft}}}{dt} + I_q \cdot \frac{d\phi_q}{dt}\right]$) represents the variation in stored magnetic energy, the last term (i.e., $\frac{3}{2}\left[\phi_d \cdot I_d - \phi_q \cdot I_q\right]$) represents the electromagnetic power transmitted from the stator to the rotor through the air gap.

The Equation of an electromagnetic torque is given by:

$$T_e = \frac{3}{2} p \cdot \left(L_d - L_q\right) \cdot I_d \cdot I_q + \frac{3}{2} \cdot p \cdot \phi_f \cdot I_q \tag{11}$$

Where ϕ_f is the permanent magnet flux linkage [Wb].
The machine rotor is considered to have sliding poles, i.e., $\left(L_d = L_q\right)$. Consequently, the expression (11) is simplified as follows:

$$T_e = \frac{3}{2} \cdot p \cdot I_q \cdot \phi_f \tag{12}$$

The conversion of electrical energy to mechanical energy in the PMSM is expressed by the following Equation:

$$J \cdot \frac{d\Omega}{dt} + f_r \cdot \Omega = T_e - T_r \tag{13}$$

By replacing the Equation (12) in Equation (13). this gives :

$$\frac{d\Omega}{dt} = \frac{3 \cdot p \cdot \phi_f}{2 \cdot J} \cdot I_q - \frac{f_r}{J} \cdot \Omega - \frac{1}{J} \cdot T_r \tag{14}$$

The overall efficiency η of the PMSM is defined as the ratio of the mechanical output power to the electrical input power:

$$\eta = \frac{P_{\text{out}}}{P_{\text{in}}} = \frac{T_e \cdot \omega_m}{P_{\text{in}}} \tag{15}$$

Where P_{out} is the output mechanical power [W], P_{in} is the input electrical power [W], T_e is the electromagnetic torque [Nm], ω_m is the angular speed [rad/s]

Electrical input power Equation:

$$P_{\text{in}} = \frac{3}{2} \cdot (v_d i_d + v_q i_q) \tag{16}$$

Where v_d, v_q is the voltage in the dq-axis, i_d, i_q is the current components in the dq-axis reference frame

Total losses Equation:

$$P_{\text{loss}} = P_{\text{Cu}} + P_{\text{Fe}} + P_{\text{mech}} + P_{\text{add}} \tag{17}$$

Where P_{add} is the additional losses (Stray, Harmonic, PWM)

The copper losses (stator winding losses):

$$P_{\text{Cu}} = 3 \cdot R_s \cdot (i_d^2 + i_q^2) \tag{18}$$

Where R_s is the resistance per phase of the stator winding [Ω]

The iron losses (core losses):

$$P_{\text{Fe}} = k_h \cdot f \cdot B^2 + k_e \cdot f^2 \cdot B^2 \tag{19}$$

Where k_h is the hysteresis loss coefficient, f is the frequency [Hz], k_e is the eddy current loss, B is the magnetic flux density in the iron core [T].

The mechanical losses (Friction & Windage):

$$P_{\text{mech}} = B_m \cdot \omega_m^2 + F \cdot \omega_m \tag{20}$$

Where B_m is the windage loss coefficient, F is the friction loss coefficient.

VI. RESULTS AND DISCUSSIONS

The curves shown in the Figures 3 to 6 reflect the dynamic variations of torque, stranded losses, and currents where the results are compared between the IPMSMs with demagnetization fault and the healthy IPMSM using Maxwell 2D software. The obtained results illustrated in Figures 7 and 8 indicate an analysis of the magnetic flux density distributions, magnetic flux intensity, and flux lines, which are intended to evaluate the electromagnetic behavior of the various IPMSM components. Based on the data extracted from this analysis, the efficiency and loss maps shown in Figures 9 to 10 were calculated and generated, which provide a thorough estimation of the motor's behavior under various operating conditions and the fault's impact on the overall system functioning.

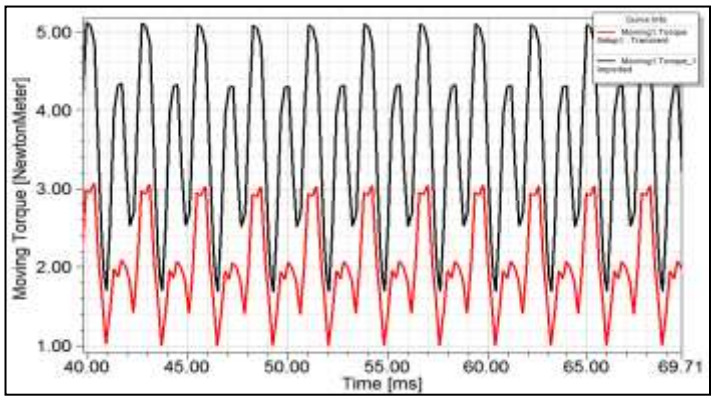

Figure 3: Torque curves variations of the IPMSMs.
Source: Authors, (2025).

In Figure 3, the black curve indicates the torque of the IPMSM in the healthy state, exhibiting a consistent and regular pattern in the range of 2 to 5 Nm and an average torque of approximately 3.7 - 3.8 Nm, with limited steady ripples indicating a balanced distribution of magnetic flux inside the rotor. In contrast, the red curve of the faulty IPMSM exhibits a sharp reduction in torque between 1 and 3 Nm, with an average torque of about 1.5 - 1.6 Nm, and the ripple in the red curve is noticeable and severe, indicating a perturbation in the magnetic flux causing an increase in mechanical vibrations and noise, which indicates the effect of demagnetization on the stability and operational efficiency of the IPMSM.

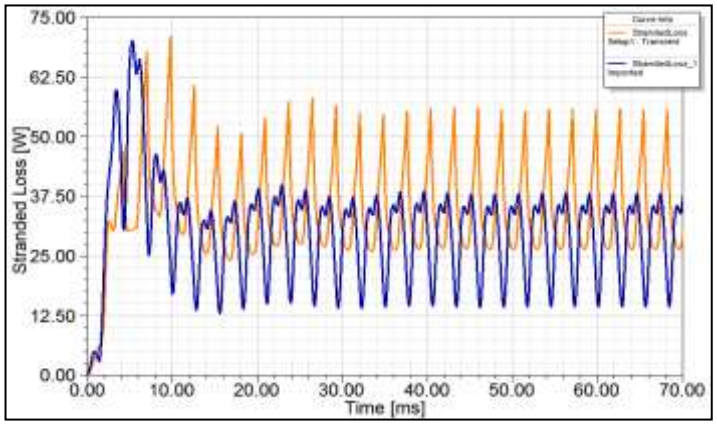

Figure 4: The IPMSMs stranded losses.
Source: Authors, (2025).

As illustrated in Figure 4, which shows the stranded losses curves of the IPMSM, the affected demagnetized machine (orange curve) exhibits a noticeable and continuous increase in losses compared to the healthy IPMSM (blue curve). While the losses in the healthy state settle within a steady range between 15 and 37 watts in the shape of periodic waves, reflecting the stability of the internal magnetic field and balanced currents, in the faulty state they exceed 50 watts with sharp oscillations, reflecting the disturbance of the magnetic field and increased compensating currents in the stator windings to compensate for the reduced flux. This increase in losses is directly attributed to the decrease in flux due to the permanent magnets degradation, which leads to an increase in the currents applied to the stator currents to compensate for the decrease in flux, thereby increasing the losses. These results confirm that continued monitoring of stranded losses curves is an effective means for early detection of demagnetization failure in the IPMSM, allowing for improved system reliability and failure avoidance.

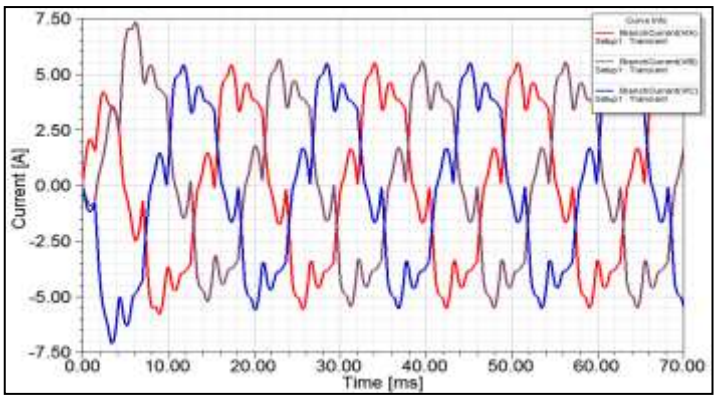

Figure 5: Healthy IPMSM current.
Source: Authors, (2025).

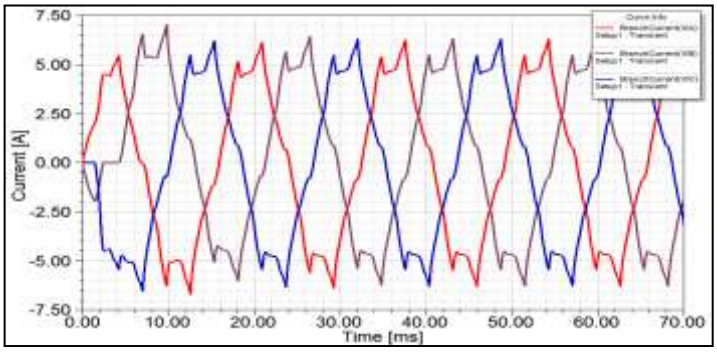

Figure 6: Current of IPMSM under demagnetization fault.
Source: Authors, (2025).

Figures 5 and 6 show a comparison of the branch current curves of the IPMSM in the cases of healthy operation and demagnetization failure, exhibiting a distinct difference in the shape and temporal behavior of the currents. In the healthy state, the currents are regularly alternating between the three branches, reflecting a balanced system and a steady magnetic flux inside the machine. On the other hand, the defective case reveals noticeable distortions in the waveform, with steeper slopes currents, an increase in the maximum current values, and relatively greater peaks and troughs compared to the healthy case, indicating that the system is injecting higher currents to compensate for the flux loss due to weakened magnets, as well as overlapping harmonic components and a slight misalignment of currents. Harmonic interference and a slight phase imbalance, which may affect the IPMSM operation and increase the torque ripple, as a results of the weak magnetic flux caused by the deterioration of the permanent magnets To compensate for this decrease in flux, the inverter is forced to drive higher currents, which increases the deformation in the current form. This negatively affects the efficiency and stability of the machine. Therefore, the branches currents analysis indicates a malfunction in the system and contributes to the early diagnosis of faults in the IPMSM.

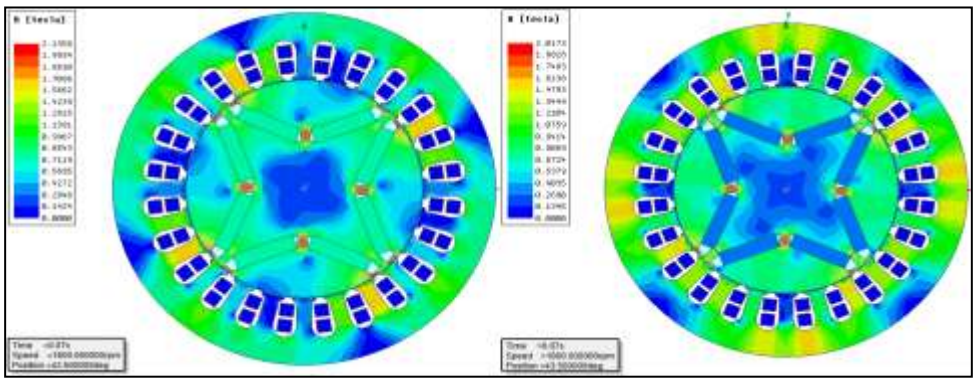

(a) (b)

Figure 7: Distribution of the magnetic flux density: a) Healthy IPMSM, b) IPMSM under demagnetization fault.
Source: Authors, (2025).

The magnetic flux density of the healthy IPMSM in Figure 7a exhibits a homogenous and uniform distribution, reflecting stable magnetic field behavior and high efficiency in power and torque conversion. In contrast, in the defective IPMSM in Figure 7b, the permanent magnet's magnetic flux density is significantly reduced to 0.4 Tesla while in the healthy IPMSM it reaches 0.8 Tesla. Irregular flux density distribution is observed in other machine parts with the appearance of regions of reduced flux between the air gap and the permanent magnets due to the loss of their effectiveness, while the magnetic saturation appears in the rotor between the magnets and the stator as well as more saturation in the stator, this disruption leads to a decrease in efficiency, power conversion, and increase in torque ripples.

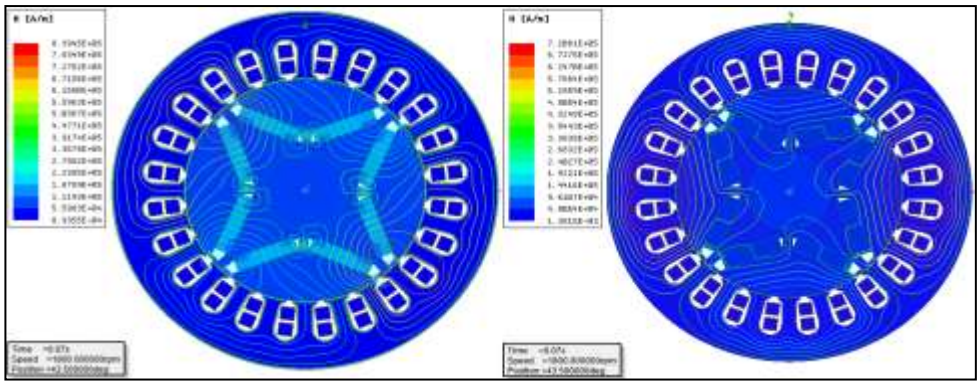

(a) (b)

Figure 8: Distribution of the magnetic intensity and flux lines: a) Healthy IPMSM, b) IPMSM under demagnetization fault.
Source: Authors, (2025).

Figure 8 indicates that the magnetic intensity and the flux lines of a healthy IPMSM exhibit a homogeneous and uniform field distribution, with consistent and uniform magnetic flux lines, reflecting high efficiency and the strength of the magnetic connection between the rotor and the stator. In contrast, a demagnetization fault leads to a decrease in magnetic field strength in each permanent magnet as well as deformation and irregularity of the flux lines, causing magnetic imbalance inside the machine, reduced operating efficiency and torque instability, highlighting the importance of electromagnetic analysis in the early detection of this type of failure.

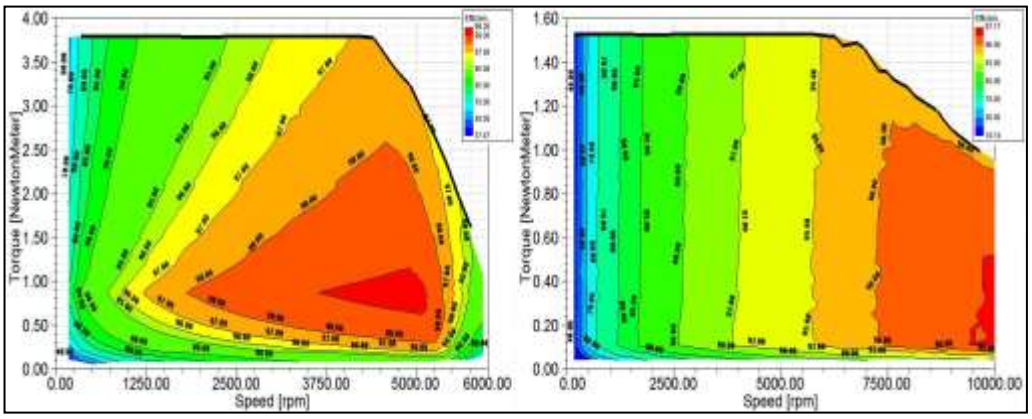

(a) (b)

Figure 9: Efficiency Maps: a) Healthy IPMSM, b) IPMSM under demagnetization fault.
Source: Authors, (2025).

The efficiency map of the IPMSM after the demagnetization failure shows an overall degradation in performance. In the case of a healthy IPMSM, there is a distinct concentration of high efficiency areas greater than 97% over an effective operational range between 1250 and 5500 rpm and torques up to 3.8 Nm, with a wide spread of high efficiency areas indicating a magnetic balance and consistent flux distribution inside the rotor. After the demagnetization, the highest recorded efficiency decreases to 97% and the highest efficiency above 96% is confined to a range of speeds between 7300 to 10000 rpm and a lower torque of 0.1 to 1.1 Nm. The efficiency decreases at lower speeds and over most areas of the map. The expansion of the speed range to 10000 rpm in case of failure is due to the torque drops drastically and attempting to compensate the loss through expansion of the operating range. The decrease in efficiency is attributed to the deterioration of magnetic flux due to the weakening effect of permanent magnets after the demagnetization, increased losses in the iron core and windings, torque deformation, and a reduction in power conversion.

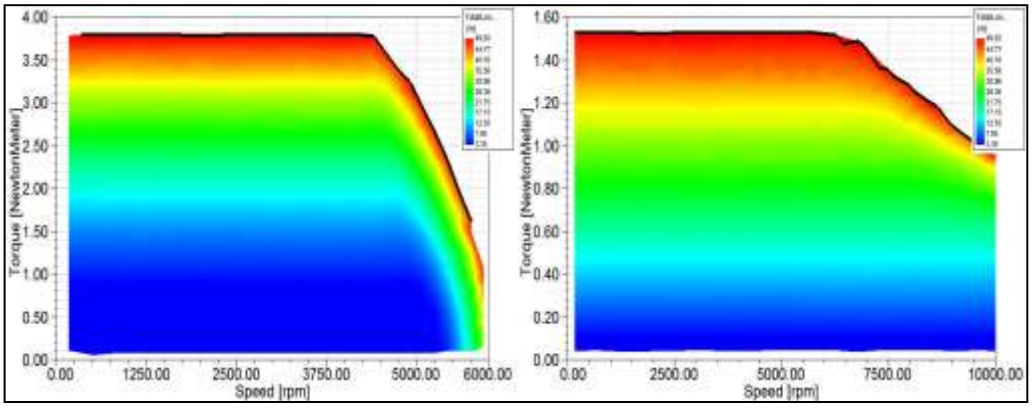

(a) (b)

Figure 10: Loss maps: a) Healthy IPMSM, b) IPMSM under demagnetization fault.
Source: Authors, (2025).

The loss map of the IPMSM after the demagnetization, in Figure 10b, indicates a significant alteration in the performance characteristics compared to the healthy IPMSM. The faulty machine exhibits a sharp decrease in the torque producing ability, The maximum operating peak torque is reduced by 57 % from 3.8 Nm in the healthy machine to 1.55 Nm, in the healthy IPMSM in Figure 10a, the losses increase in a tight range between 3.2 and 3.8 torques. While in the case of partial demagnetization failure, the maximum operating range at 1.2 to 1.55 Nm , and the speed range extends to 10000 rpm, this comes at the expense of the ability to generate a higher torque, which reduces the overall efficiency.

The degradation in functioning is due to the reduction in flux resulting from the loss of magnetic material properties, which leads to lower magnetic flux density in the air gap and reduced electromotive force (EMF). As a result, the IPMSM requires higher currents to compensate for the lack of torque, which increases the copper losses. The absence of magnetization affects the positioning of the optimal operating point in the MTPA curve, resulting in inefficient operation outside the maximum efficiency area. On the other hand, Iron losses increases as the operational frequencies increase at higher speeds. Thus, it can be considered that partial demagnetization leads to a profound disruption of the torque and the efficiency in the IPMSM, which hinders the stability of operation in high torque applications and requires the adoption of strategies for early detection and compensation in intelligent control systems.

VII. CONCLUSIONS

In this paper, the effect of partial demagnetization faults on the IPMSM behavior is investigated by relying on the efficiency and loss maps compared to a healthy IPMSM. The results indicate that these faults deteriorate the efficiency of the machine under various operating conditions, particularly in the high torque and speed areas, with large ripples and a significant reduction in torque affecting the maximum safety threshold for operation. The results emphasize the importance of monitoring the condition of permanent magnets based on data extracted from the efficiency maps and the advanced electromagnetic analysis, for early detection of the demagnetization faults, which can lead to system degradation, increased losses, reduced efficiency, significant loss in power conversion effectiveness, the appearance of magnetic saturation in certain parts of the machine and inconsistent flux distribution, which emphasizes the importance of early detection of this failure type. The analysis of the magnetic field distribution reveals complex distortions in the magnetic flux density and intensity that affect the overall machine functioning and highlights the reliance on the advanced analysis based on efficiency maps for in-depth investigation of the impact of these failures. This contributes to the enhancement of predictive maintenance systems for electric motors. These systems increase reliability and reduce maintenance costs.

VIII. AUTHOR'S CONTRIBUTION

Conceptualization: Layachi Chebabhi, Toufik Tayeb Naas, Mohamed Zitouni, Monaem Elmnifi and Abdelkarim Cherhabil.
Methodology: Layachi Chebabhi, Toufik Tayeb Naas, Mohamed Zitouni, Monaem Elmnifi and Abdelkarim Cherhabil.
Investigation: Layachi Chebabhi, Toufik Tayeb Naas, Mohamed Zitouni, Monaem Elmnifi and Abdelkarim Cherhabil.
Discussion of results: Layachi Chebabhi, Toufik Tayeb Naas, Mohamed Zitouni, Monaem Elmnifi and Abdelkarim Cherhabil.
Writing – Original Draft: Layachi Chebabhi, Toufik Tayeb Naas, Mohamed Zitouni, Monaem Elmnifi and Abdelkarim Cherhabil.
Writing – Review and Editing: Layachi Chebabhi, Toufik Tayeb Naas, Mohamed Zitouni, Monaem Elmnifi and Abdelkarim Cherhabil.
Resources: Layachi Chebabhi, Toufik Tayeb Naas, Mohamed Zitouni, Monaem Elmnifi and Abdelkarim Cherhabil.
Supervision: Layachi Chebabhi, Toufik Tayeb Naas, Mohamed Zitouni, Monaem Elmnifi and Abdelkarim Cherhabil.
Approval of the final text: Layachi Chebabhi, Toufik Tayeb Naas, Mohamed Zitouni, Monaem Elmnifi and Abdelkarim Cherhabil.

IX. REFERENCES

[1] Djaloul Karboua, Toufik Mebkhouta, Youcef Chouiha, Abdelkader Azzeddine Bengharbi, B. ouadeh Douara, and Belgacem Toual, "Enhancing Performance of Permanent Magnet Synchronous Motor Drives Through Hybrid Feedback Linearization and Sliding Mode Control," ITEGAM- Journal of Engineering and Technology for Industrial Applications (ITEGAM-JETIA), vol. 10, no. 49, pp. 178–186, Jan. 2024, doi: https://doi.org/10.5935/jetia.v10i49.1222.

[2] M. O. Mustafa and G. S. Mohammed, "Design of Particle Swarm Optimization-Based PID Controller for High-Performance PMSM Speed Control," ITEGAM-Journal of Engineering and Technology for Industrial Applications (ITEGAM-JETIA), vol. 11, no. 53, pp. 216–224, Jan. 2025, doi: https://doi.org/10.5935/jetia.v11i53.2024.

[3] Touahria D, Bouchemha A, Kahla S. Design and simulation of hybrid system PV/PEMFC/Battery/Super Capacitor powered PMSM motor for electric vehicle. Sebha University Conference Proceedings 2025; 4 (1): 176–181. doi: https://doi.org/10.51984/sucp.v4i1.3976.

[4] Nouraldin NA, Chebaani M, Számel L, Abdelwahab SAM, Abdellatif WS. Experimental investigation of predictive control for PMSM-based wind turbine generation system. Computers and Electrical Engineering 2024; 119: 109554. doi: https://doi.org/10.1016/j.compeleceng.2024.109554.

[5] Számel L, Nouraldin NA, Chebaani M, Abdelwahab SAM, Abdellatif WS. Experimental investigation of predictive control for PMSM-based wind turbine generation system. SSRN 2024. doi: https://doi.org/10.2139/ssrn.4871457.

[6] Sonandkar S, Selvaraj R, Chelliah TR. PV powered improved quasi-Z-source inverter fed five-phase PMSM for marine propulsion systems. IEEE Transactions on Transportation Electrification 2024; 11 (1): 393–403. doi: https://doi.org/10.1109/tte.2024.3391615.

[7] Karthik K, Ponnambalam P. Design and implementation of time-based fault tolerance technique for solar PV system reliability improvement in different applications. Scientific Reports 2025; 15 (1): 7377. doi: https://doi.org/10.1038/s41598-025-91464-4.

[8] Zhao W, Cheng M, Ji J, Cao R, Du Y, Li F. Design and analysis of a new fault-tolerant linear permanent-magnet motor for maglev transportation applications. IEEE Transactions on Applied Superconductivity 2012; 22 (3): 5200204. doi: https://doi.org/10.1109/tasc.2012.2185209.

[9] Karboua D, Belgacem T, Khan ZH, Kellal C. Robust performance comparison of PMSM for flight control applications in more electric aircraft. PLoS ONE 2023; 18 (7): e0283541. doi: https://doi.org/10.1371/journal.pone.0283541.

[10] Zhang C, Zhang X, Zhao F, Gerada D, Li L. Improvements on permanent magnet synchronous motor by integrating heat pipes into windings for solar unmanned aerial vehicle. Green Energy and Intelligent Transportation 2022; 1 (1): 100011. doi: https://doi.org/10.1016/j.geits.2022.100011.

[11] Lamichhane A, Zhou L, Yao G, Luqman M. Modeling, control and power management of six-phase PMSM based shipboard MVDC distribution system. Energies 2020; 13 (16): 4229. doi: https://doi.org/10.3390/en13164229.

[12] Kim SA. A study on the predictive maintenance algorithms considering load characteristics of PMSMs to drive EGR blowers for smart ships. Energies 2021; 14 (18): 5744. doi: https://doi.org/10.3390/en14185744.

[13] Hong DK, Joo DS, Lee JY, Woo BC. Effects of the pole-slot combination on the PMSM of an integrated motor propulsor for an unmanned underwater vehicle considering its electric performance, noise and vibration. Int J Appl Electromagn Mech 2016; 52 (3–4): 1689–1695. doi: https://doi.org/10.3233/jae-162162.

[14] Chen W, Mao Z, Tian W. Water cooling structure design and temperature field analysis of permanent magnet synchronous motor for underwater unmanned vehicle. Applied Thermal Engineering 2024; 240: 122243. doi: https://doi.org/10.1016/j.applthermaleng.2023.122243.

[15] Yang Y, He Q, Fu C, Liao S, Tan P. Efficiency improvement of permanent magnet synchronous motor for electric vehicles. Energy 2020; 213: 118859. doi: https://doi.org/10.1016/j.energy.2020.118859.

[16] Yuan T, Wang D, Wang X, Wang X, Sun Z. High-precision servo control of industrial robot driven by PMSM-DTC utilizing composite active vectors. IEEE Access 2019; 7: 7577–7587. doi: https://doi.org/10.1109/access.2018.2890539.

[17] S. C. Vanamala and K. K. Danduprolu, “Speed Control of PMSM drive using Model Predictive Control Based Field Oriented Control,” ITEGAM- Journal of Engineering and Technology for Industrial Applications (ITEGAM-JETIA, vol. 11, no. 52, 2025, doi: https://doi.org/10.5935/jetia.v11i52.1243.

[18] Bilgin O, Kazan FA. The effect of magnet temperature on speed, current and torque in PMSMs. In: 2016 XXII International Conference on Electrical Machines (ICEM); 2016 Sep; pp. 2080–2085. IEEE. doi: https://doi.org/10.1109/icelmach.2016.7732809.

[19] Shi C, Peng L, Zhang Z, Shi T. Analytical modeling and analysis of permanent-magnet motor with demagnetization fault. Sensors 2022; 22 (23): 9440. doi: https://doi.org/10.3390/s22239440.

[20] Vlachou VI, Karakatsanis TS. Development of a fault-tolerant permanent magnet synchronous motor using a machine-learning algorithm for a predictive maintenance elevator. Machines 2025; 13 (5): 427. doi: https://doi.org/10.3390/machines13050427.

[21] Amira Amira Slimani, Amor Bourek, A. Ammar, Khoudir Kakouche, Wassila Hattab, and M. Bacha, “Artificial Neural Network-Based Deadbeat Predictive Current Control with Dead-Time Compensation for PMSMs,” ITEGAM- Journal of Engineering and Technology for Industrial Applications (ITEGAM-JETIA), vol. 11, no. 51, Jan. 2025, doi: https://doi.org/10.5935/jetia.v11i51.1456.

[22] S.-C. Wang, Y.-C. Nien, and S.-M. Huang, “Multi-Objective Optimization Design and Analysis of V-Shape Permanent Magnet Synchronous Motor,” Energies, vol. 15, no. 10, p. 3496, May 2022, doi: https://doi.org/10.3390/en15103496.

[23] M. Ayaz, Yiğit Karabulut, Serkan Aktaş, and Erkan Meşe, “Electromagnetic Design and Comparative Analysis of Compact PM Motors for Ventricular Assist Devices,” Physica Scripta, vol. 100, no. 8, pp. 085019–085019, Jul. 2025, doi: https://doi.org/10.1088/1402-4896/adf401.

[24] Y.-J. Lee, Y.-C. Chang, and Y.-L. Lim, “Design and Performance Evaluation of High-Efficiency SiC Interior Permanent Magnet Synchronous Motor Drive Systems,” 2022 IEEE Industry Applications Society Annual Meeting (IAS), pp. 1–6, Jun. 2025, doi: https://doi.org/10.1109/ias62731.2025.11061490.

[25] Chebabhi L, Naas TT, Zitouni M. Comparative study of 2D designs of 12/8 and 10/8 switched reluctance motors using ANSYS Maxwell. ITEGAM-JETIA 2025; 11 (52): 186–195. doi: https://doi.org/10.5935/jetia.v11i52.1604.

[26] Chebabhi L, Naas TT, Zitouni M, Ghibeche I, Benmessaoud T. Influence of choosing materials on 6/4 switched reluctance motor performance. Studies in Engineering and Exact Sciences 2024; 5 (1): 2391–2406. doi: https://doi.org/10.54021/seesv5n1-118.

[27] J. de las Morenas, L. M. Belmonte, and R. Morales, “Streamlined Bearing Fault Detection Using Artificial Intelligence in Permanent Magnet Synchronous Motors,” Machines, vol. 13, no. 5, p. 357, Apr. 2025, doi: https://doi.org/10.3390/machines13050357.

[28] A. H. Baharvand, S. Hossein Beigi Fard, A. H. Poursaeed, and M. Doostizadeh, “An optimized classifier chains-based deep learning framework for Inter-Turn Fault diagnosis in Permanent Magnet Synchronous Motors,” Applied Soft Computing, vol. 180, p. 113482, Jun. 2025, doi: https://doi.org/10.1016/j.asoc.2025.113482.

[29] A. Sergakis, M. Salinas, N. Gkiolekas, and K. N. Gyftakis, “A Review of Condition Monitoring of Permanent Magnet Synchronous Machines: Techniques, Challenges and Future Directions,” Energies, vol. 18, no. 5, p. 1177, Feb. 2025, doi: https://doi.org/10.3390/en18051177.

[30] Wu S, Ma G, Yao C, Sun Z, Xu S. Current sensor fault detection and identification for PMSM drives using multichannel global maximum pooling CNN. IEEE Transactions on Power Electronics 2024; 39 (8): 10311–10325. doi: https://doi.org/10.1109/tpel.2024.3395290.

[31] Wu Y, Zhang J, Xu Z, Wang S, Fu H. Feature extraction and applicability comparisons for fault detection of inter-turn short-circuited PMSM. IEEE Transactions on Instrumentation and Measurement 2024; 73: 1–10. doi: https://doi.org/10.1109/tim.2024.3509588.

[32] Goktas T, Zafarani M, Akin B. Discernment of broken magnet and static eccentricity faults in permanent magnet synchronous motors. IEEE Transactions on Energy Conversion 2016; 31 (2): 578–587. doi: https://doi.org/10.1109/tec.2015.2512602.

[33] Pindoriya RM, Gautam G, Rajpurohit BS. A novel application of pseudorandom-based technique for acoustic noise and vibration reduction of PMSM drive. IEEE Transactions on Industry Applications 2020; 56 (5): 5511–5522. doi: https://doi.org/10.1109/tia.2020.2997904.

[34] Wang YS, Guo H, Yuan T, Ma LF, Wang C. Electromagnetic noise analysis and optimization for permanent magnet synchronous motor used on electric vehicles. Engineering Computations 2021; 38 (2): 699–719. doi: https://doi.org/10.1108/ec-02-2020-0070.

[35] Pietrzak P, Wolkiewicz M. Demagnetization fault diagnosis of permanent magnet synchronous motors based on stator current signal processing and machine learning algorithms. Sensors 2023; 23 (4): 1757. doi: https://doi.org/10.3390/s23041757.

[36] Huang W, Du B, Li T, Cheng Y, Cui S. Detection of PMSM demagnetization fault and eccentricity fault based on acoustic images and DeiT classifier. IEEE Transactions on Energy Conversion 2025. doi: https://doi.org/10.1109/tec.2025.3550544.

[37] Meiwei Z, Weili L, Haoyue T. Demagnetization fault diagnosis of the permanent magnet motor for electric vehicles based on temperature characteristic quantity. IEEE Transactions on Transportation Electrification 2022; 9 (1): 759–770. doi: https://doi.org/10.1109/tte.2022.3200927.

[38] Lale T, Yüksek G. Identification and classification of turn short-circuit and demagnetization failures in PMSM using LSTM and GRU methods. Bull Pol Acad Sci Tech Sci 2025; 73 (1). doi: https://doi.org/10.24425/bpasts.2024.151958.

[39] Chen H, Gao C, Si J, Nie Y, Hu Y. A novel method for diagnosing demagnetization fault in PMSM using toroidal-yoke-type search coil. IEEE Transactions on Instrumentation and Measurement 2021; 71: 1–12. doi: https://doi.org/10.1109/tim.2021.3134991.

[40] Yu Y, Gao H, Chen Q, Liu P, Niu S. Demagnetization fault detection and location in PMSM based on correlation coefficient of branch current signals. Energies 2022; 15 (8): 2952. doi: https://doi.org/10.3390/en15082952.

[41] Zhang Q, Cui J, Xiao W, Mei L, Yu X. Demagnetization fault diagnosis of a PMSM for electric drilling tools using GAF and CNN. Electronics 2024; 13 (1): 189. doi: https://doi.org/10.3390/electronics13010189.

[42] Ruoho S, Arkkio A. Partial demagnetization of permanent magnets in electrical machines caused by an inclined field. IEEE Transactions on Magnetics 2008; 44 (7): 1773–1778. doi: https://doi.org/10.1109/tmag.2008.921951.

[43] Li Z, Zhao S, Yang X, Cao J, Li J. Partial demagnetization fault diagnosis of interior permanent magnet synchronous motor based on back electromotive force constant of a new search coil. IEEE Transactions on Instrumentation and Measurement 2025. doi: https://doi.org/10.1109/tim.2025.3585215.

[44] Ding S, Wang X, Li Y, Wu Z, Hang J. Online diagnosis of partial demagnetization fault in PMSMs based on kurtosis of air-gap flux density signal difference. IEEE Transactions on Power Electronics 2025. doi: https://doi.org/10.1109/tpel.2025.3580750.

[45] Xing Z, Wang X, Zhao W, Chen A, Yu S. Analysis and improvement of reliability of surface-mounted permanent magnet synchronous motors based on subdivision subdomain models. IEEE Transactions on Energy Conversion 2025. doi: https://doi.org/10.1109/tec.2025.3573783.

[46] Hanselman DC. Brushless permanent magnet motor design. The Writers' Collective; 2003.

[47] Hendershot JR, Miller TJE. Design of brushless permanent-magnet motors. Oxford University Press; 1995. Available: https://academic.oup.com/book/52967

[48] Dexter Magnetic Technologies. Available at: https://www.dextermag.com/products/permanent-magnets/neodymium-iron-boron-magnets/

[49] MAGNET SOP. Mathematical modeling and simulation of permanent magnet synchronous motor. Int J Adv Res Electr Electron Instrum Eng 2013; 2 (8).

[50] Roshen W. Iron loss model for permanent-magnet synchronous motors. IEEE Transactions on Magnetics 2007; 43 (8): 3428–3434. doi: https://doi.org/10.1109/tmag.2007.899687.